

mAbs

Taylor & Francis

ISSN: 2256-6688

ISSN: (Print) (Online) Journal homepage: <https://www.tandfonline.com/loi/kmab20>

# Multivalent design of the monoclonal SynO2 antibody improves binding strength to soluble $\alpha$ -Synuclein aggregates

Inga Petersen, Muhammad Ilyas Ali, Alex Petrovic, Anders Jimmy Ytterberg, Karin Staxäng, Monika Hodik, Fadi Rofo, Sina Bondza & Greta Hultqvist

**To cite this article:** Inga Petersen, Muhammad Ilyas Ali, Alex Petrovic, Anders Jimmy Ytterberg, Karin Staxäng, Monika Hodik, Fadi Rofo, Sina Bondza & Greta Hultqvist (2023) Multivalent design of the monoclonal SynO2 antibody improves binding strength to soluble  $\alpha$ -Synuclein aggregates, mAbs, 15:1, 2256668, DOI: [10.1080/19420862.2023.2256668](https://doi.org/10.1080/19420862.2023.2256668)

**To link to this article:** <https://doi.org/10.1080/19420862.2023.2256668>



© 2023 The Author(s). Published with license by Taylor & Francis Group, LLC.



View supplementary material [↗](#)



Published online: 22 Sep 2023.



Submit your article to this journal [↗](#)



Article views: 851



View related articles [↗](#)



View Crossmark data [↗](#)



REPORT



# Multivalent design of the monoclonal SynO2 antibody improves binding strength to soluble $\alpha$ -Synuclein aggregates

Inga Petersen<sup>a</sup>, Muhammad Ilyas Ali<sup>a</sup>, Alex Petrovic<sup>a</sup>, Anders Jimmy Ytterberg<sup>b</sup>, Karin Staxäng<sup>c</sup>, Monika Hodik<sup>c</sup>, Fadi Rofo<sup>a</sup>, Sina Bondza<sup>d,e</sup>, and Greta Hultqvist<sup>d</sup>

<sup>a</sup>Department of Pharmacy, Uppsala University, Uppsala, Sweden; <sup>b</sup>Department of Pharmacy, SciLifeLab Drug Discovery and Development, Uppsala University, Uppsala, Sweden; <sup>c</sup>TEM Laboratory, BioVis Platform, Uppsala University, Uppsala, Sweden; <sup>d</sup>Ridgeview Instruments AB, Uppsala, Sweden; <sup>e</sup>Department of Immunology, Genetics and Pathology, Uppsala University, Uppsala, Sweden

## ABSTRACT

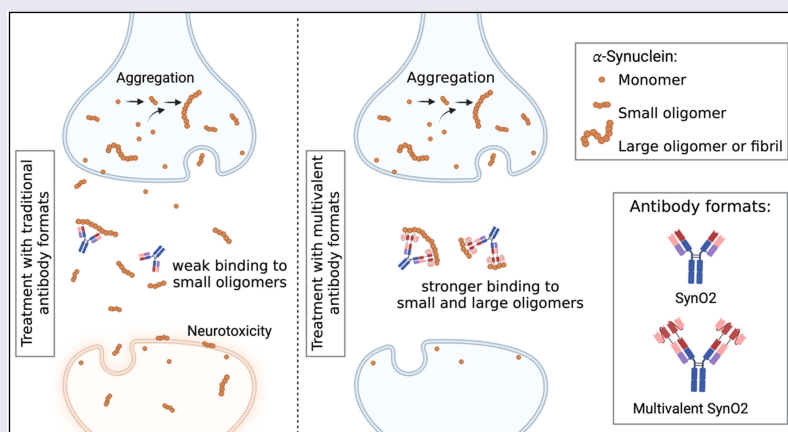
Soluble aggregates are reported to be the most neurotoxic species of  $\alpha$ -Synuclein ( $\alpha$ Syn) in Parkinson's disease (PD) and hence are a promising target for diagnosis and treatment of PD. However, the predominantly intracellular location of  $\alpha$ Syn limits its accessibility, especially for antibody-based molecules and prompts the need for exceptionally strong soluble  $\alpha$ Syn aggregate binders to enhance their sensitivity and efficacy for targeting the extracellular  $\alpha$ Syn pool. In this study, we have created the multivalent antibodies TetraSynO2 and HexaSynO2, derived from the  $\alpha$ Syn oligomer-specific antibody SynO2, to increase avidity binding to soluble  $\alpha$ Syn aggregate species through more binding sites in close proximity. The multivalency was achieved through recombinant fusion of single-chain variable fragments of SynO2 to the antibodies' original N-termini. Our ELISA results indicated a 20-fold increased binding strength of the multivalent formats to  $\alpha$ Syn aggregates, while binding to  $\alpha$ Syn monomers and unspecific binding to amyloid  $\beta$  protofibrils remained low. Kinetic analysis using LigandTracer revealed that only 80% of SynO2 bound bivalently to soluble  $\alpha$ Syn aggregates, whereas the proportion of TetraSynO2 and HexaSynO2 binding bi- or multivalently to soluble  $\alpha$ Syn aggregates was increased to ~95% and 100%, respectively. The overall improved binding strength of TetraSynO2 and HexaSynO2 implies great potential for immunotherapeutic and diagnostic applications with targets of limited accessibility, like extracellular  $\alpha$ Syn aggregates. The ability of the multivalent antibodies to bind a wider range of  $\alpha$ Syn aggregate species, which are not targetable by conventional bivalent antibodies, thus could allow for an earlier and more effective intervention in the progression of PD.

## ARTICLE HISTORY

Received 20 March 2023  
Revised 1 September 2023  
Accepted 5 September 2023

## KEYWORDS



Avidity; multivalent antibodies; Parkinson's disease (PD); soluble aggregates; alpha-Synuclein ( $\alpha$ Syn)




## Introduction

Aggregation and intracellular deposition of alpha-Synuclein ( $\alpha$ Syn) are the main characteristics of neurodegenerative synucleinopathies, of which Parkinson's disease (PD) is the most common. Whether  $\alpha$ Syn aggregation is the disease's cause or the result of another underlying dysfunction is not

fully understood, but the presence of  $\alpha$ Syn aggregates in early presymptomatic PD stages and its contribution to the severe loss of dopaminergic neurons in the substantia nigra is widely accepted.<sup>1</sup> The diagnosis of PD is still mostly carried out through the assessment of motor dysfunction.<sup>2</sup>

**CONTACT** Greta Hultqvist  [greta.hultqvist@farmaci.uu.se](mailto:greta.hultqvist@farmaci.uu.se)  Department of Pharmacy, Uppsala University, Husargatan 3, Uppsala 75123, Sweden

 Supplemental data for this article can be accessed online at <https://doi.org/10.1080/19420862.2023.2256668>

© 2023 The Author(s). Published with license by Taylor & Francis Group, LLC.

This is an Open Access article distributed under the terms of the Creative Commons Attribution License (<http://creativecommons.org/licenses/by/4.0/>), which permits unrestricted use, distribution, and reproduction in any medium, provided the original work is properly cited. The terms on which this article has been published allow the posting of the Accepted Manuscript in a repository by the author(s) or with their consent.



However, by the time PD becomes symptomatic approximately 30–50% of nigral dopaminergic neurons are already lost. Current medical treatments for PD patients compensate for the dopamine deficiency, but no disease-modifying treatment is available.

$\alpha$ Syn is located inside the pre-synaptic terminals of neurons as either disordered cytoplasmic monomers or helical membrane-bound monomers or multimers.<sup>3–6</sup> Under physiological conditions,  $\alpha$ Syn is presumably involved in the regulation of neurotransmitter release by acting as a chaperone on the SNARE (soluble N-ethylmaleimide-sensitive fusion protein attachment protein receptors) complex assembly.<sup>4</sup> In PD pathology,  $\alpha$ Syn aggregation is best described by the nucleation-conversion-polymerization model,<sup>7,8</sup> where misfolded  $\alpha$ Syn initiates nucleation, promoting a clustering of misfolded  $\alpha$ Syn and resulting in oligomer formation. Evidence suggests that the oligomers have anti-parallel  $\beta$ -sheet, i.e., hairpins,<sup>9–11</sup> which twist to become parallel ordered  $\beta$ -sheet structures upon fibril formation.<sup>7,12,13</sup> These fibrils exist in many different sizes and are predominantly insoluble, whereas oligomers are generally considered soluble.<sup>8,14</sup>

Many studies suggest that small  $\alpha$ Syn oligomers are the most neurotoxic  $\alpha$ Syn species, causing membrane perturbation,<sup>15</sup> synaptic dysfunction,<sup>16</sup> oxidative stress,<sup>17,18</sup> mitochondrial dysfunction<sup>19</sup> and neuronal inflammation.<sup>20,21</sup>  $\alpha$ Syn fibrils might also cause toxicity through the release of oligomers and seed further aggregation.<sup>14</sup> It is likely that all  $\alpha$ Syn species, monomers, oligomers and fibrils alike, are secreted by neurons to some degree and are partly found extracellularly.<sup>22</sup> Extracellular  $\alpha$ Syn oligomers and fibrils are reported to be taken up by phagocytic cells<sup>23,24</sup> as well as by neurons, which has been suggested to contribute to the spread of  $\alpha$ Syn pathology.<sup>14,25,26</sup> Therefore, therapeutically targeting both  $\alpha$ Syn oligomers and fibrils to reduce their toxicity and propagation has a high potential.

Utilizing antibodies as binders to  $\alpha$ Syn aggregates offers high target specificity and affinity and has therefore been studied extensively for diagnostic and therapeutic applications in PD. Several antibodies targeting  $\alpha$ Syn oligomers and fibrils have reached Phase 1 and Phase 2 clinical trials.<sup>27–31</sup> These antibodies have been reported to reduce soluble plasma  $\alpha$ Syn levels and slow down PD pathology in *in vitro* and *in vivo* models,<sup>32</sup> but no therapeutic effect in humans has been observed in clinical trials thus far.<sup>33</sup>

High affinity binding of IgG antibodies to aggregates is in most cases achieved by avidity, i.e., the combined binding strength of multiple binding sites on one target molecule. Despite the small amount of  $\alpha$ Syn extracellularly available for antibody binding, enhancing an antibody's binding strength to soluble  $\alpha$ Syn aggregates beyond bivalency could improve its sensitivity and efficacy for diagnostic and therapeutic applications by increasing the duration of antibody–target association. We have previously designed multivalent antibodies with the aim to increase the avidity to amyloid beta ( $A\beta$ ) aggregates,<sup>34,35</sup> where the hexavalent Hexa-RmAb158, derived from the antibody RmAb158 (murine version of lecanemab)<sup>36</sup>, showed an at least 40-fold stronger binding to  $A\beta$  protofibrils larger than 100 kDa compared to the bivalent RmAb158.<sup>35</sup>

In this study, we adopted the same multivalent antibody designs for the production of high-avidity  $\alpha$ Syn aggregate-targeting antibodies, namely TetraSynO2 and HexaSynO2. Our designs are based on the antibody SynO2, which is reported to bind to  $\alpha$ Syn oligomers and fibrils with a 27,000-fold higher affinity compared to monomers.<sup>37</sup> Maintaining this low affinity to monomers is important to preserve the physiological function of monomeric  $\alpha$ Syn<sup>38</sup> and to minimize the risk of  $\alpha$ Syn-antibody complexes being carried from the blood into the brain.

We show here that TetraSynO2 and HexaSynO2 exhibit increased avidity to soluble  $\alpha$ Syn aggregates compared to SynO2, while retaining a low affinity to  $\alpha$ Syn monomers, making the multivalent antibodies promising candidates for future diagnostic and treatment of PD.

## Results

### Generation of antibodies

To increase avidity of SynO2 to  $\alpha$ Syn oligomers and fibrils, single-chain variable fragments (scFv) of SynO2 were recombinantly fused to the N-terminal ends of each SynO2 heavy and light chain, forming HexaSynO2, or fused to only the N-terminal of the heavy chain, forming TetraSynO2 (Figure 1 a). The scFvSynO2 were recombinantly constructed from the SynO2 heavy and light chain variable domains linked together via a (G<sub>4</sub>S)<sub>3</sub> linker. HexaSynO2, TetraSynO2 and the parental SynO2, used as a control, were expressed and purified yielding approximately 15 mg of SynO2, 2 mg of TetraSynO2 and 1 mg of HexaSynO2 per liter of transfected cell culture. SDS-PAGE analysis confirmed the size and purity of the purified antibodies, with SynO2 presenting as one band at 150 kDa, TetraSynO2 presenting as one band at ~200 kDa and HexaSynO2 presenting as one band at ~260 kDa (Figures 1b and S1). The heavy and light chains are clearly represented under reducing conditions, with the TetraSynO2 and HexaSynO2 having an expected elevated heavy chain molecular weight (MW) or heavy and light chain MW, respectively, compared to SynO2 (Figures 1 and S1).

### Recombinant fusion of scFvSynO2 on SynO2 minimally decreases thermal stability

The addition of domains to an antibody can cause a change in its structural properties. We therefore tested the structural stability in increasing heat of SynO2, TetraSynO2 and HexaSynO2 using the Tycho nt.6 system. SynO2 showed high inflection temperatures of 74.4°C and 81.8°C (Figure 2), indicating a high structural stability. TetraSynO2 and HexaSynO2 gave very similar, but slightly lower first inflection temperatures of 70.2°C and 70.0°C, respectively (Figures 2 and S3). The lower inflection temperatures are likely due to the additional scFvs, which unfold at lower temperatures.<sup>35,39</sup> However, the inflection temperatures are still relatively high, suggesting a high structural stability and an overall antibody-like folding of the tetra- and hexavalent antibody formats.



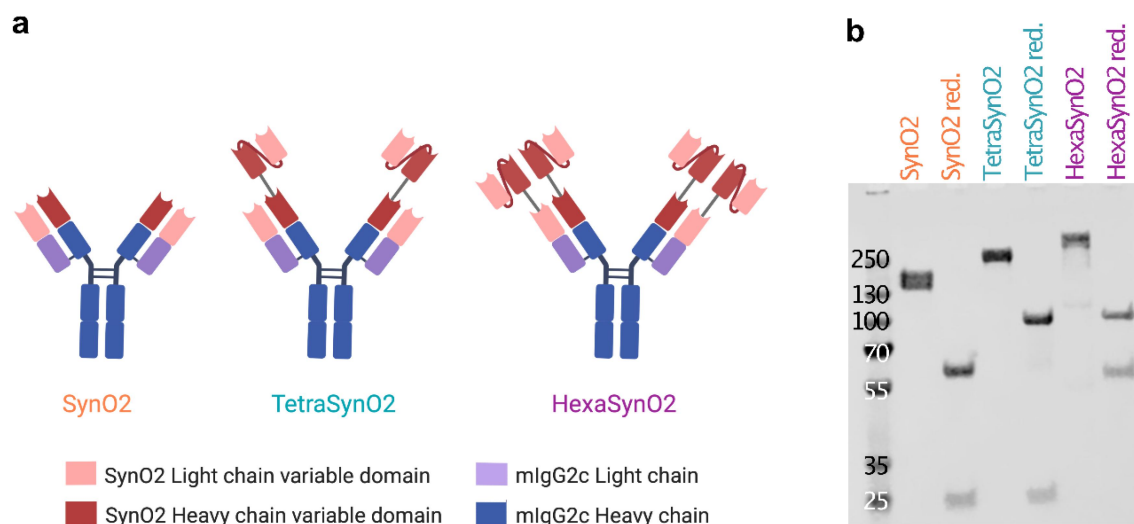


**Figure 1.** Design of recombinantly produced antibodies. (a) Schematic illustration of the parental antibody SynO2, TetraSynO2 and HexaSynO2 with scFvSynO2 recombinantly fused to the N-termini of heavy and/or light chains of SynO2. (b) SDS-PAGE with Coomassie staining of antibodies loaded under non-reducing and reducing (red.) conditions. Bands of intact antibodies under non-reducing conditions appear at approximately 150 kDa for SynO2, 200 kDa for TetraSynO2 and 260 kDa for HexaSynO2 (1  $\mu$ g protein/lane).

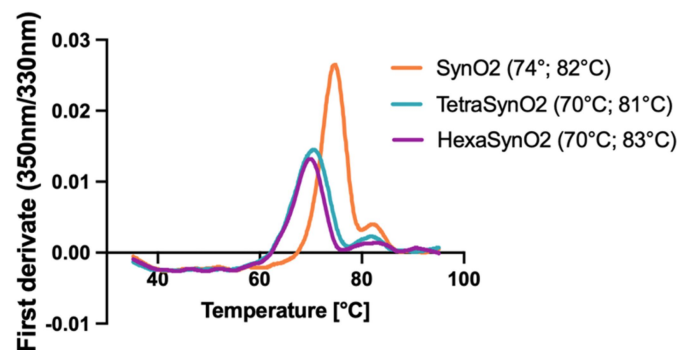


**Figure 2.** Thermal stability of SynO2, TetraSynO2 and HexaSynO2 measured by Tycho. First derivate of ratio between intrinsic fluorescence measured at 350 nm and 330 nm, while the antibodies were heated up linearly from 35°C to 95°C. Inflection temperatures, visible as peaks, represent major unfolding events at 74°C and 82°C for SynO2, 70°C and 81°C for TetraSynO2 and 70°C and 83°C for HexaSynO2, suggesting high structural stability for all three antibodies.

### SynO2 selectivity for $\alpha$ Syn aggregates is based on avidity

By creating TetraSynO2 and HexaSynO2 we aimed to increase the overall binding strength toward  $\alpha$ Syn aggregates through enhanced avidity effects. We started out by determining whether the binding strength of SynO2 to aggregated  $\alpha$ Syn is mediated by bivalent engagement of the antibody. To answer this question, we generated antigen-binding fragments (Fabs) of SynO2 (SynO2Fab) (Figure 3a) and compared their binding strength to  $\alpha$ Syn aggregates, prepared by incubation with 4-hydroxy-2-nonenal (HNE), with the full SynO2 antibody in an indirect ELISA (Figure 3b, c). Coomassie-stained SDS-PAGE showed bands at the expected size for the freshly biotinylated SynO2 and SynO2Fab at 150 kDa and 50 kDa, respectively (Figure 3a). The indirect ELISA results showed approximately 100-fold weaker binding of SynO2Fab to  $\alpha$ Syn HNE aggregates compared to the full antibody SynO2 (Figure 3c). These results suggest that avidity is crucial for the  $\alpha$ Syn aggregate binding of SynO2.

### HexaSynO2 binds amyloid beta aggregates weakly

Aggregated  $\alpha$ Syn shares properties with other amyloid proteins regarding their  $\beta$ -sheet secondary structure. To demonstrate that the high affinity of HexaSynO2 is not caused by an increased affinity toward a random structural element present in any amyloid aggregate, we tested its binding to A $\beta$  aggregates present in Alzheimer's disease using a sandwich ELISA with A $\beta$ 42 protofibrils captured by an A $\beta$ 42 C-terminal-specific antibody (Figure 4a). The results showed that both SynO2 and HexaSynO2 bind to A $\beta$ , but only when applied at elevated concentrations (Figure 4b). HexaSynO2 had slightly stronger binding to A $\beta$ , compared to SynO2, but still demonstrated a 100-fold weaker binding when compared to the A $\beta$  aggregate-specific antibody RmAb158. Despite having weak binding to A $\beta$  aggregates, these results suggest an unspecific mode of binding of SynO2 and HexaSynO2 to A $\beta$  aggregates.

### HexaSynO2 has a higher apparent affinity to $\alpha$ Syn HNE aggregates than SynO2

As HexaSynO2 features more  $\alpha$ Syn binding sites than SynO2, we expected it to have increased binding strength to  $\alpha$ Syn HNE aggregates and  $\alpha$ Syn fibrils due to increased avidity compared to SynO2. An inhibition ELISA setup (Figure 5a) was chosen to detect differences in the binding strength of these antibodies. In contrast to classic indirect ELISA setups, the inhibition ELISA has the advantage of incubating the antibodies with  $\alpha$ Syn in solution, which resembles a more physiologically relevant situation. Additionally, binding signals in classic ELISAs are measured after long incubation times of the antibody with its target to achieve a binding equilibrium and are therefore not sensitive enough to detect significant differences in binding strength between very strong binders.

With the inhibition ELISA we observed a 34-fold and 43-fold stronger binding of HexaSynO2 to  $\alpha$ Syn HNE aggregates and  $\alpha$ Syn fibrils, respectively, when compared to SynO2. Both,



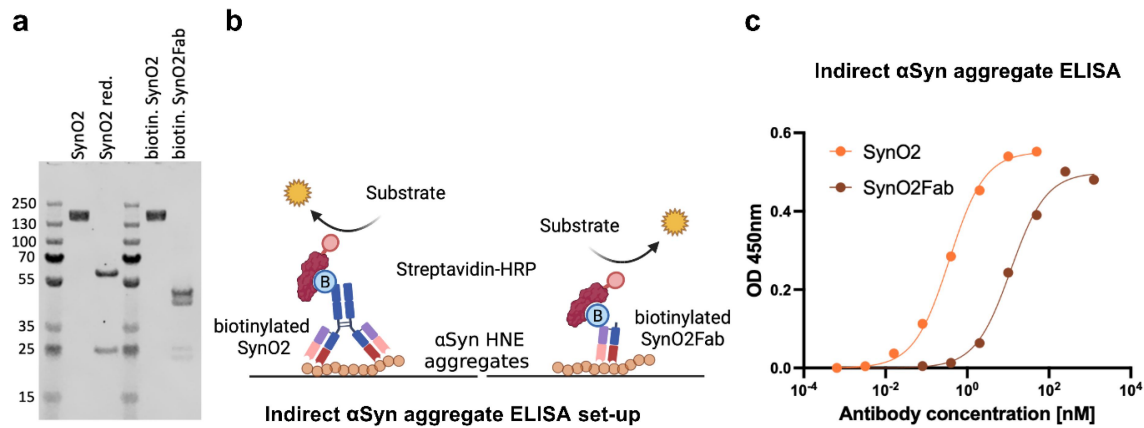


**Figure 3.** Characterization of SynO2Fab. (a) Coomassie-stained SDS-PAGE shows a band at 150 kDa for biotinylated SynO2 and a band at 50 kDa for the biotinylated SynO2Fab. 1 µg protein/lane. The complete gel can be seen in Figure S6. (b) Schematic illustration of the indirect αSyn aggregate ELISA set-up with biotinylated SynO2 or biotinylated SynO2Fab binding to the αSyn HNE aggregate coating and detection by Streptavidin-horseradish peroxidase (HRP). (c) Indirect αSyn aggregate ELISA binding curves show strong binding by SynO2 to αSyn HNE aggregates and weak binding by SynO2Fab. The degree of biotinylation of SynO2 and SynO2Fab was compared by direct ELISA (Figure S7) and was verified by liquid chromatography–mass spectrometry (Figure S8-9, Tables S1-3).

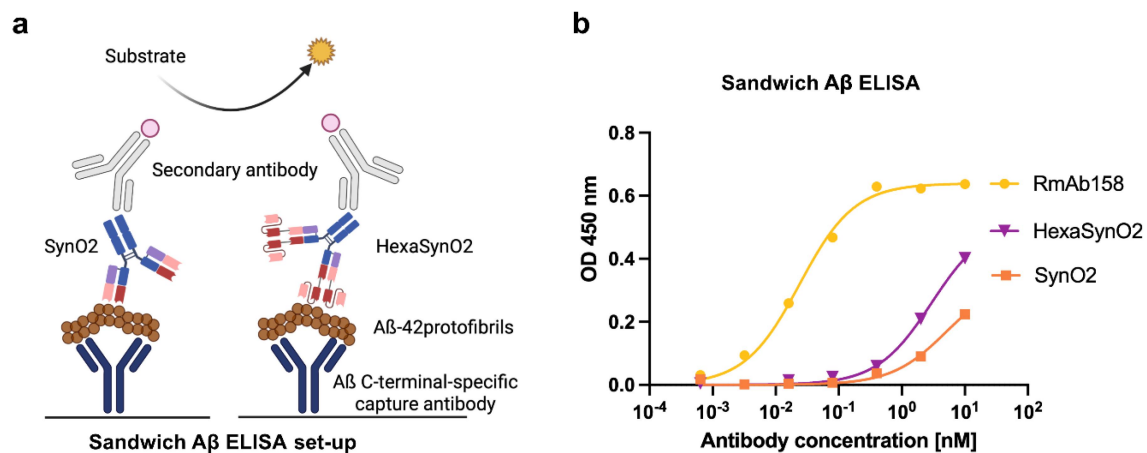


**Figure 4.** Sandwich Aβ ELISA detects cross-reactivity of SynO2 and HexaSynO2 with Aβ aggregates. (a) Schematic illustration of the sandwich Aβ ELISA set-up with Aβ42 protofibrils captured by an Aβ C-terminal-specific antibody coated to a plate. Binding of SynO2, HexaSynO2 and RmAb158 was detected through an HRP-conjugated secondary antibody. (b) Sandwich ELISA binding signal demonstrating unspecific binding of SynO2 and HexaSynO2 to Aβ42 protofibrils at high antibody concentrations. Nonlinear regression curves (“one site – specific binding”) were calculated in GraphPad Prism.

SynO2 and HexaSynO2 exhibited very low binding to αSyn monomers (Figure 5b). The binding strength was measured as the half-maximal inhibitory concentrations (IC<sub>50</sub>), which is defined as the concentration of target proteins in the pre-incubation mixture at which 50% of the antibodies are inhibited from binding to the target immobilized on the plate (Figure 5b).

#### **TetraSynO2 and HexaSynO2 dissociate slower from αSyn HNE aggregates than SynO2**

LigandTracer assays were conducted to test whether the increased affinity of the multivalent antibody format to αSyn HNE aggregates, as seen in the inhibition ELISA, leads to a decreased dissociation rate as expected if it has achieved increased avidity. Compared to other techniques measuring protein binding kinetics, such as surface plasmon resonance, LigandTracer allows the determination of the kinetics of very strong interactions, as protein dissociations can be measured

over an extended period of time. Iodine-125 (<sup>125</sup>I)-labeled antibodies were applied to αSyn HNE aggregate-coated dishes at two different concentrations consecutively to achieve more accurate calculations of the kinetic parameters. The dissociation kinetics were subsequently measured after all unbound antibodies were removed (Figure 6a).

Different kinetic models were used to evaluate the kinetic parameters of each interaction. The interaction of SynO2Fab with αSyn HNE aggregates was well described by a “one-to-one depletion corrected” interaction model. Correction for ligand depletion was justified by the theoretical ratio of αSyn HNE aggregates to SynO2Fab being 5:1 at the highest ligand concentration, which was also visible in the rapid curve saturation in both association phases (Figure 6b). The dissociation rate constant ( $k_d$ ) calculated for SynO2Fab using the “one-to-one depletion corrected” model was  $2.37 \times 10^{-4} \text{ s}^{-1}$ , reflecting the  $k_d$  of a monovalent interaction (Figure 6b).

For the interaction of the full SynO2 antibody with αSyn HNE aggregates, we observed a biphasic dissociation for which



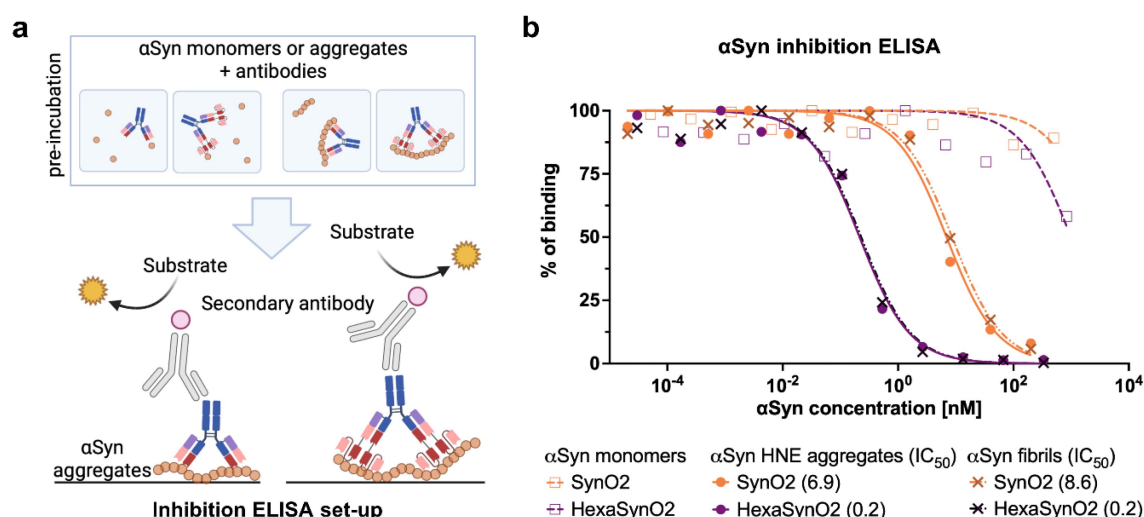


**Figure 5.** Inhibition ELISA illustrating the binding strength of SynO2 and HexaSynO2 to αSyn monomers, HNE aggregates and αSyn fibrils. (a) Schematic illustration of the αSyn inhibition ELISA set-up, with SynO2 or HexaSynO2 pre-incubated with αSyn monomers, αSyn HNE aggregates or αSyn fibrils, and subsequently added to an αSyn HNE aggregate-coated plate. (b) Visualization of binding signals, normalized to 0% as no signal and 100% as the maximal signal of each construct, respectively. Linear regression curves (“log(inhibitor) vs. normalized response”) were calculated in GraphPad Prism. IC<sub>50</sub> values, calculated from the regression curves, indicate the concentration of αSyn HNE aggregate or αSyn fibrils needed in solution with the antibody to inhibit 50% of the respective antibody from binding to the αSyn HNE aggregate-coated surface.

a “one-to-one” interaction model was not sufficient. The biphasic dissociation indicates a heterogeneous interaction with overlapping weak (monovalent) and strong (bivalent) components, which has been shown to be best described by using a “one-to-two” interaction model.<sup>40</sup> Here, the  $k_d$  calculated for the weaker of the two interaction components of SynO2 was  $4.14 \times 10^{-4} \text{ s}^{-1}$ , which coincides with the affinity calculated for the monovalent SynO2Fab, indicating that this weak interaction component of SynO2 is a monovalently binding cohort of antibody molecules. The  $k_d$  of the stronger interaction component of SynO2 was calculated to be at least  $1.35 \times 10^{-6} \text{ s}^{-1}$ , which is a 300-fold slower  $k_d$  than the weak interaction component (Figures 6b and S10a). The strong interaction component likely represents a cohort of SynO2 that binds bivalently to the target, contributing approximately  $80 \pm 4\%$  to the overall binding.

The interaction of TetraSynO2 with αSyn HNE aggregates also showed a partially biphasic dissociation, though with a smaller cohort of quickly dissociating antibodies. Using a “one-to-two” model with the kinetic parameters for the weaker interaction component set constant to the association rate constant ( $k_a$ ) and  $k_d$  values obtained with SynO2Fab resulted in a  $k_d$  of at least  $1.37 \times 10^{-6} \text{ s}^{-1}$  for the stronger interaction component, similar to the  $k_d$  obtained for the bivalently binding SynO2 cohort (Figures 6c and S10b). Similar kinetic values were obtained for TetraSynO2 using a “one-to-one” model, indicating that the cohort of TetraSynO2 antibodies binding monovalently represents only a minor fraction. The contribution of avidity enhanced binding to the overall binding of TetraSynO2 was estimated to be  $95 \pm 2\%$ .

HexaSynO2 showed a homogeneous, stable interaction with αSyn HNE aggregates with nearly no dissociation, indicating that all antibodies bound bi- or multivalently to the target. We used a “one-to-one depletion corrected” model for the kinetic evaluation, which resulted in similar kinetic parameters as

a “one-to-one” model, indicating that ligand depletion is only present to a minor extent, but described the interaction curve of the first association phase more accurately. The calculated  $k_d$  of at least  $1.51 \times 10^{-6} \text{ s}^{-1}$  was again similar to the values seen with the strong interaction components of TetraSynO2 and SynO2 (Figure 6c).

However, we cannot exclude that the true dissociation rates of the strong interaction components, presented above, are even slower. Since the slowest dissociation rates that we could measure here resulted in a horizontal dissociation line, dissociation rates slower than that could not be distinguished. Even if the kinetic evaluation were run with the dissociation rates locked to  $10^{-8} \text{ s}^{-1}$ , we achieved equally good fitting curves. Hence, the dissociation rates for the strong interaction components presented here should be considered at least in the range of  $10^{-6} \text{ s}^{-1}$ , but could be stronger.

In conclusion, the LigandTracer results support our hypothesis presented above (Figure 3c) that SynO2 binds αSyn HNE aggregates strongly, due to its ability to bind them with higher avidity. The increased avidity in the multivalent antibody formats decreases their dissociation from the target even further and increases the cohort size of antibodies being able to bind bi- or multivalently to αSyn HNE aggregates.

## Discussion

Here, we developed the tetravalent antibody, TetraSynO2, and the hexavalent antibody, HexaSynO2, with the aim to increase the avidity of SynO2 to αSyn aggregates, such as oligomers and fibrils. We thereby intended to target a higher amount of soluble αSyn aggregates using the same antibody dose. Previously, a similar multivalent antibody design was successfully used with the Aβ aggregate-specific antibody RmAb158.<sup>34,35</sup>

SynO2, the antibody that we based the multivalent antibody designs upon, was originally reported to bind conformation-



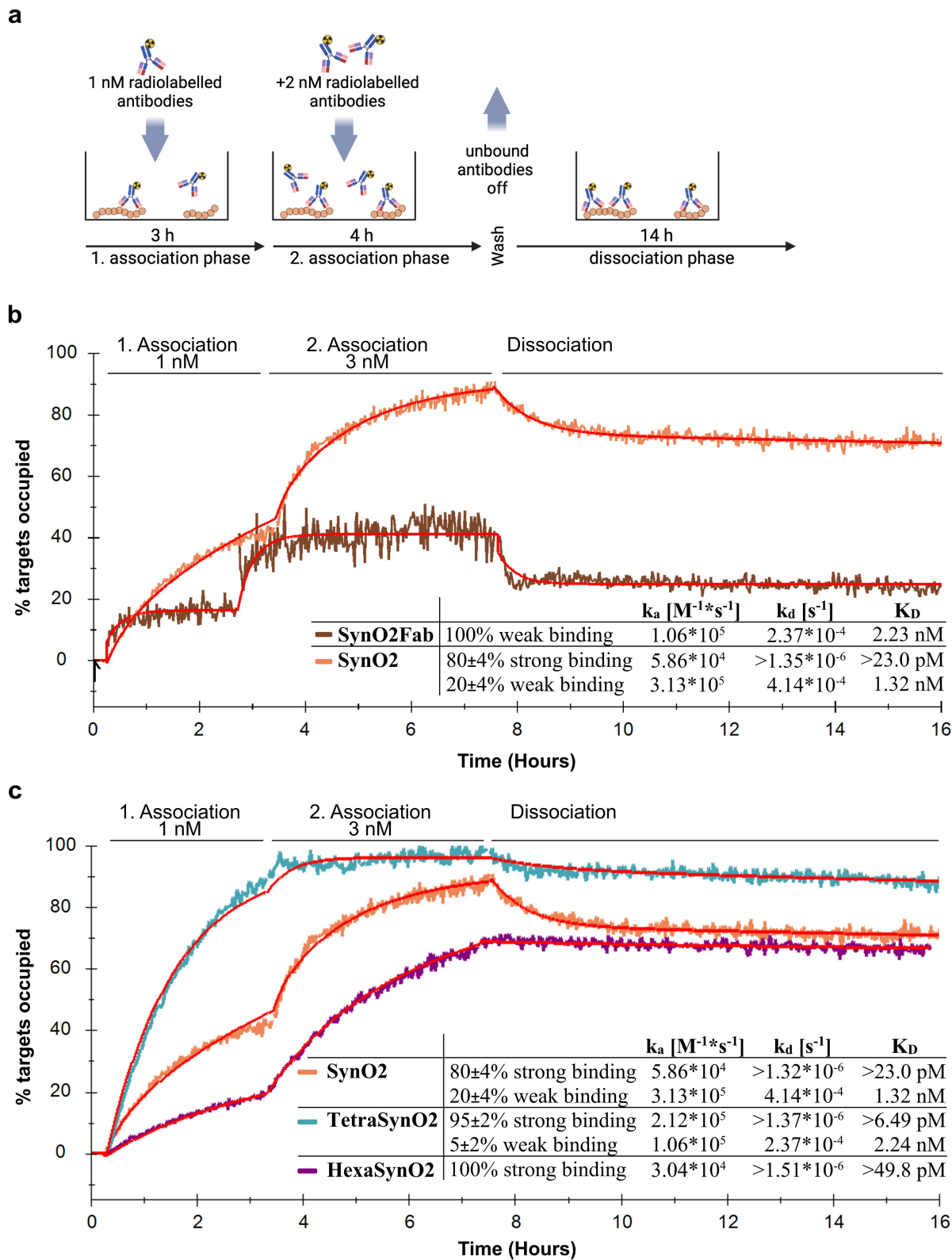


**Figure 6.** Kinetic evaluation of interactions of SynO2Fab, SynO2, TetraSynO2 and HexaSynO2 with  $\alpha$ Syn HNE aggregates recorded by LigandTracer. (a) Schematic illustration of the LigandTracer set-up with a plastic surface coated with  $\alpha$ Syn HNE aggregates and  $^{125}I$ -labelled antibodies added in solution. (b) Interaction curves of SynO2Fab and SynO2, and (c) SynO2, TetraSynO2 and HexaSynO2 with  $\alpha$ Syn HNE aggregates recorded by LigandTracer and fitting curves (red) using a one-to-one depletion corrected model (SynO2Fab, HexaSynO2) or a one-to-two model (SynO2, TetraSynO2), respectively. 100 nM coating with  $\alpha$ Syn HNE aggregates. Two consecutive association phases (3 hours and 4 hours, respectively) with 1 nM and 3 nM of the respective  $^{125}I$ -labelled antibody. Recorded interaction curves were evaluated in TraceDrawer using a “one-to-one depletion corrected” (SynO2Fab and HexaSynO2) or a “one-to-two” model (SynO2 and TetraSynO2). Signal intensities of each curve were scaled to Bmax, the estimated signal intensity at saturation, with 100% representing target saturation.



specific  $\alpha$ Syn oligomers and that the  $\alpha$ Syn C-terminal was part of the antibody's epitope.<sup>37</sup> By ELISA and LigandTracer assays, we showed that the monovalent SynO2Fab had a much lower affinity to  $\alpha$ Syn HNE aggregates compared to the full antibody. Furthermore, our inhibition ELISA results showed that SynO2 had almost identical affinities to  $\alpha$ Syn HNE aggregates and  $\alpha$ Syn fibrils, which both appeared structurally very different in transmission electron microscopy analysis (Fig. S4e). Thus, our findings suggest that the specificity of SynO2 toward  $\alpha$ Syn aggregates is dependent upon avidity binding, rather than depending solely on a structural epitope.<sup>41</sup> Increasing the number of binding sites and having them in close proximity, as in TetraSynO2 and HexaSynO2, should further increase the antibodies' avidity to  $\alpha$ Syn aggregates, assuming that the aggregates are large enough to accommodate bivalent binding of the antibodies to the same aggregate at the same time.

For a detailed characterization of the binding kinetics, we carried out LigandTracer experiments for which the  $\alpha$ Syn HNE aggregates had to be immobilized to the dish surface. The coating concentration was aimed at the lower range of 100 nM (1.4  $\mu$ g/ml), but still high enough to ensure good signal/noise ratio. Under these experimental conditions, we could show that the proportion of antibodies binding bi- or multivalently to  $\alpha$ Syn HNE aggregates increased from  $80 \pm 4\%$  for the parental antibody SynO2 to  $95 \pm 2\%$  for TetraSynO2 and estimated close to 100% for HexaSynO2, based upon the contribution of the strong interaction component to the overall interaction (Figure 6c). We defined the strong interaction components for TetraSynO2 and HexaSynO2 by their slow dissociation rate, which were calculated to be at least 170- or 300-fold higher, respectively, compared to the dissociation rate calculated for the weak interaction components. Hence, the additional scFvSynO2 in TetraSynO2 and HexaSynO2 allowed proportionally more antibodies to bind bi- or multivalently to  $\alpha$ Syn HNE aggregates. With the antibody Hexa-RmAb158, we have previously shown that the additional binding sites and their close proximity in the hexavalent format not only increased the antibody's binding strength to large A $\beta$  aggregates compared to the bivalent RmAb158, but also enabled strong binding to small A $\beta$  oligomers, to which RmAb158 had only weak affinity.<sup>35</sup> Similar to Hexa-RmAb158, we also expect HexaSynO2 to offer more flexibility to the antibody, allowing it to bind conformations and sizes of  $\alpha$ Syn aggregates that would sterically not be accessible to SynO2.

We could not accurately measure any interaction stronger than bivalent binding with our experimental set-up, as the slowest dissociation rate for bivalent interactions was calculated to be in the range of  $10^{-6} \text{ s}^{-1}$  and already resulted in a horizontal line during dissociation. All dissociation rates calculated here for the strong interaction components should therefore be considered at least as slow as stated, if not slower. Hence, it was not possible for us to draw any further conclusion about the valency of the interaction other than distinguishing between monovalent and any higher valency binding. In contrast to the substantial changes observed for the dissociation

rates, the association rates varied only to a minor degree between the different antibody formats and interaction components, implying similar molecular target recognition, and therefore indicating that the same epitope is recognized.

For cases where multivalent binding establishes quickly relative to the measurement time, the 1:2 model presents a suitable approach to distinguish the antibody fractions that engage in monovalent versus multivalent binding. The 1:2 model assumes the presence of two independent 1:1 interactions, which is not entirely accurate for discriminating between the monovalent and avidity enhanced binding.<sup>40</sup> For multivalent binders the number of available target epitopes decreases faster than predicted for a 1:1 interaction, which is reflected in a seemingly slower on-rate. This is one of the reasons why the strong binding components, which represent bi- or multivalent interactions, have lower  $k_a$ -values compared to the weaker, monovalent interactions. Another factor contributing to the small differences in association rates is that the binder is either a scFv of SynO2 or an original variable domain without additional linkers. Adding an amino acid linker between the variable heavy and light chain of an antibody to generate an scFv can result in structural changes and has been reported previously to alter its affinity compared to the antibody's original binding site.<sup>42</sup> Therefore, the use of scFvSynO2 as binding sites in TetraSynO2 and HexaSynO2 could explain the slight decrease in molecular recognition observed for the multivalent constructs. For HexaSynO2, the initial binding event is more likely to occur through a scFvSynO2, since it has relatively more scFvs than original binding sites. It is also likely that the two original  $\alpha$ Syn binding sites on HexaSynO2 are partly sterically hindered by the attached scFvs, and therefore are less accessible to participate in  $\alpha$ Syn aggregate binding, which might also explain the lower  $k_a$ -value observed for the multivalent binding fraction. In TetraSynO2, however, the original binding sites are likely to be more accessible, as the scFv are only attached to the heavy chain, which may be the reason why TetraSynO2 exhibits a slightly higher  $k_a$ -value for the multivalent fraction compared to HexaSynO2.

In conclusion, the limited amount of  $\alpha$ Syn aggregates present extracellularly, along with the wide spectrum of  $\alpha$ Syn aggregates sizes and structures, poses a challenge in targeting the propagation of toxic  $\alpha$ Syn aggregates in the brain. By avidity-enhanced binding, traditional bivalent antibody formats can discriminate well between physiologically important monomeric and pathological aggregated targets, but may fail to bind with avidity to all different aggregate species. Here we have shown that by introducing additional binding sites to the antibody SynO2, the proportion of antibodies binding by avidity to  $\alpha$ Syn aggregates was improved to approximately 100%, resulting in even stronger binding. This study underlines the importance of a detailed evaluation and understanding of the antibody binding kinetics when dealing with a limited and diverse target pool. With their enhanced binding strength to large  $\alpha$ Syn moieties, the multivalent antibodies TetraSynO2 and HexaSynO may have an improved



diagnostic and therapeutic potential against  $\alpha$ Syn aggregation, spreading, and toxicity.

## Material and methods

### *Antibody cloning, expression and purification*

scFv of the SynO2 antibody were designed with an internal ( $G_4S$ )<sub>3</sub> linker and recombinantly fused with a 20 amino acid linker (RADAAPGGGSGGGTVSIFPP) to the N-terminus of the variable region of both heavy and light chain of the parental SynO2 antibody to generate a hexavalent antibody, HexaSynO2. The genes for heavy and light chain were cloned into pcDNA3.4 vectors (GeneArt, Regensburg, Germany). Antibodies were expressed by transient transfection in Expi293 cells as described previously<sup>43</sup>. In brief, vectors for light and heavy chain were transfected at a ratio of 7:3 with polyethyleneimine (PEI) (Polysciences 24,765–1) as a transfection agent. Seven days post-transfection, cell culture supernatants were filtered through a 0.22  $\mu$ m filter (Millipore GPW04700) and antibodies were purified from the supernatant by affinity chromatography using a protein G column (Cytiva GE17-0404-01). Antibodies eluted at approx. 70% elution buffer (0.7% acetic acid). Purified antibodies were concentrated using a 30K MWCO Amicon Ultra-15 centrifugal filter unit (Millipore UFC9030) and the buffer was changed to phosphate-buffered saline (PBS) using a 7K MWCO Zeba spin desalting column (Thermo Scientific 89,892). Protein purity was validated by analytical size exclusion chromatography (SEC), for which 10–50  $\mu$ l of antibodies in PBS (at the respective concentrations of 0.7 mg/ml for SynO2; 0.26 mg/ml for TetraSynO2 and 0.2 mg/ml for HexaSynO2) were loaded at 0.5 ml/min on a Superdex 200 Increase 10/300 GL, equilibrated with PBS, using an Äkta Go system (Cytiva, Uppsala, Sweden).

### *Protein stability analysis by Tycho*

The protein stability was analyzed using a Tycho nt.6 instrument (NanoTemper Technologies, Munich, Germany), where proteins were loaded into glass capillaries and heated up to 95°C, while their intrinsic fluorescence at 330 and 350 nm was measured. Structural changes cause changes in the amount of tyrosine and tryptophan exposed, which result in a shift in the fluorescent intensity. Major unfolding events are measured as inflection temperatures, indicated as peaks in the first derivative of the fluorescence intensity ratio 350/330 nm.

### *Fab preparation*

Fabs were generated using the Pierce Fab Micro preparation Kit (Thermo Scientific 44,685) following the manufacturer's instructions. In brief, the immobilized Papain slurry was washed and activated with Fab digestion buffer containing 20 mM cysteine pH7. The buffer of the antibodies was changed to 20 mM cysteine Fab digestion buffer using a Zeba spin desalting column 7K MWCO (Thermo Scientific 89,882). The antibodies (~0.8  $\mu$ g/ $\mu$ l concentration) were incubated

with the immobilized papain, shaking at 37°C for 15 min. The digests were separated from the immobilized papain and purified on a Nab Protein A Plus Spin Column (Thermo Scientific 89,952). The flowthroughs containing the Fabs were concentrated using a 10K MWCO Amicon Ultra-0.5 Centrifugal concentrator (Millipore UFC5003), and the buffer was exchanged to PBS using a 7K MWCO Zeba spin desalting column (Thermo Scientific 89,882). The Fab was further purified by SEC, for which the Fab in PBS was loaded at 0.5 ml/min on a Superdex 200 Increase 10/300 GL, and elution fractions corresponding to 50 kDa MW were pooled and concentrated.

### *Generation of $\alpha$ Syn HNE aggregates and $\alpha$ Syn fibrils and separation by size exclusion chromatography*

$\alpha$ Syn aggregates were prepared by incubation with HNE as described previously.<sup>44</sup> Briefly, 1 mg lyophilized  $\alpha$ Syn monomers (AnaSpec AS-55555) were dissolved to 13 mM (2 mg/ml) in 50 mM phosphate buffer pH 7.4 and centrifuged for 5 min at 21,000 $\times$ g at 4°C to remove preformed insoluble aggregates. 465  $\mu$ l of  $\alpha$ Syn monomers at 13 mM were mixed with 35  $\mu$ l of 64 mM HNE (10 mg/ml) (Cayman chemicals 32,100), vortexed for 10 s and incubated at 37°C for 72 hours without agitation. The solution was again centrifuged for 5 minutes at 21,000 $\times$ g at 4°C, and the buffer was changed to PBS using a Zeba spin desalting column 7K MWCO (Thermo Scientific 89,882).  $\alpha$ Syn fibrils were prepared by incubation of  $\alpha$ Syn monomers (AnaSpec AS-55555) (13 mM in 50 mM phosphate buffer pH 7.4) at 37°C shaking for 7 days. The  $\alpha$ Syn fibrils were centrifuged for 10 min at 21,000  $\times$  g at 4°C, and pellets, containing the insoluble fibrils, were resuspended in PBS. Single-use aliquots of  $\alpha$ Syn HNE aggregates and  $\alpha$ Syn fibrils were stored at –80°C. SEC was performed with  $\alpha$ Syn HNE aggregates to separate large and small  $\alpha$ Syn aggregates into individual fractions.  $\alpha$ Syn HNE aggregates were thawed on ice, insoluble aggregates were removed by centrifugation for 5 min at 21,000 $\times$ g at 4°C and 500  $\mu$ l protein solution were loaded on a Superdex 200 Increase 10/300 GL at a flow rate of 0.6 ml/min using the Äkta pure 25 system (Cytiva, Uppsala, Sweden). Fractions of 500  $\mu$ l were collected and analyzed by SDS-PAGE, Native PAGE and western blot.

### *Transmission electron microscopy of $\alpha$ Syn HNE aggregates and $\alpha$ Syn fibrils*

A 5  $\mu$ l drop of  $\alpha$ Syn HNE aggregates, ~1.7 mg/ml diluted 1:2 in MQ water, or  $\alpha$ Syn fibrils, ~1.7 mg/ml undiluted, was placed on a formvar- and carbon coated 200-mesh copper grid (Ted Pella). The excess solution was removed by blotting with filter paper. The sample was then directly contrasted with 2% uranyl acetate. Excess of uranyl acetate was removed by blotting on filter paper. Images were acquired on a Tecnai™ G2 Spirit BioTwin transmission electron microscope (Thermo Fisher/FEI) at 80 kV with an ORIUS SC200 CCD camera and Gatan Digital Micrograph software (both from Gatan Inc./Blue Scientific).



### SDS-PAGE and western blot analysis

The purity and size of purified proteins were determined by SDS-PAGE analysis. 1 µg purified protein was loaded with 1× LDS sample buffer (Invitrogen B0007) with or without 1× Bolt Sample reducing agent (Invitrogen B0009) on a Bolt 4 to 12% Bis-Tris 1 mm protein gel (Invitrogen NW04125) alongside a pre-stained protein marker (Thermo Scientific 26,619). The proteins were separated by size at 80 V for 1–2 hours. PAGE blue protein solution (Thermo Scientific 24,620) was used to stain for total protein. The identity of protein bands was confirmed by western blot. The proteins were transferred from the unstained SDS-PAGE gel to a PVDF membrane (Thermo Scientific 88,518) for 2 hours at 100 V using 1× Transfer buffer (Invitrogen BT00061) containing 20% methanol. The membrane was dried, reactivated in methanol and blocked with 5% skim milk and 1% Tween in Tris-buffered saline (TBS). If αSyn HNE aggregates or αSyn fibrils were blotted, an additional step to fixate aggregates on the membrane was added after reactivating the membrane, including a 30-min incubation of the membrane in 0.5% PFA in PBS. The membrane was washed in PBS, TBS-Tween, and blocked subsequently in 5% skim milk and 1% Tween in TBS. Primary and secondary antibodies chosen for the respective proteins, indicated in the respective result sections, were incubated with the membrane for 1 h. Either fluorescent signal or chemiluminescent signal from the reaction of an HRP-conjugated secondary antibody with ECL substrate (Invitrogen WP20005) was recorded with the Odyssey Fc Imaging system (LI-COR Biosciences, Lincoln, NE). Signal intensity analysis was carried out using ImageStudio Lite Software (LI-COR Biosciences, Lincoln, NE).

### Native PAGE analysis

Native PAGE was performed to analyze the protein size under non-denaturing conditions. 1–2 µg purified protein was loaded with 1× Native PAGE sample buffer (Invitrogen BN2003) on a NativePAGE 4 to 16% Bis-Tris 1 mm protein gel (Invitrogen BN1002) alongside an unstained protein standard (Invitrogen LC0725). 1× Native PAGE running buffer as anode buffer and 1× Native PAGE running buffer with 1:200 diluted Native PAGE cathode additive as cathode buffer were used. The proteins were separated at 80 V for 2 hours. Native PAGE gels were destained and fixed in 40% methanol with 10% acetic acid. PAGE blue protein solution (Thermo Scientific 24,620) was used to stain for total protein. Western blot with Native PAGE was done as described above with SDS-PAGE.

### Biotinylation of antibodies

Antibodies or Fabs were biotinylated using EZ-Link™ Sulfo-NHS-Biotin (Thermo Scientific A39257) according to the manufacturers instructions. The antibody or Fab at concentrations of 0.7 mg/ml and 0.5 mg/ml, respectively, was incubated with a 50-fold molar excess of biotin for 30 min at room temperature (RT). Unbound biotin was removed using a 7K MWCO Zeba spin desalting column (Thermo Scientific 89,882) equilibrated with PBS.

### Labelling of antibodies with iodine-125

Antibodies were radioactively labeled with iodine-125 (<sup>125</sup>I) according to the Chloramine T method.<sup>45</sup> 20 µg of each antibody were mixed with 4 MBq <sup>125</sup>I (PerkinElmer Inc., Waltham, MA) and 5 µl of 1 mg/ml Chloramine-T (Sigma-Aldrich 857,319) and incubated for 90 seconds. 10 µl of 1 mg/ml sodium metabisulfite (Supelco 08982) was added to stop the reaction. The labeled antibodies were purified from free <sup>125</sup>I using a 7K MWCO Zeba spin desalting column (Thermo Scientific 89,882) equilibrated with PBS.

### Indirect ELISA to analyze avidity of SynO2 to soluble αSyn aggregates

The binding ability of SynO2 and SynO2Fab toward αSyn HNE aggregates was determined by indirect ELISA with biotinylated SynO2 and SynO2Fab. A high binding half-area 96-well plate (Corning CLS3690) was coated with 10 nM of αSyn HNE aggregates (molar concentration of monomeric units) in PBS overnight at 4°C. The following day, the coating solution was removed and the plates were blocked with 1% bovine serum albumin (BSA; Sigma-Aldrich A7030) in PBS for 2 hours shaking at RT. Serial dilutions of the antibodies were prepared in ELISA incubation buffer (0.1% BSA, 0.05% Tween-20 in PBS), with a starting concentration of 10 nM for SynO2 or 1000 nM for SynO2Fab, and incubated on the plate for 2-hour shaking at RT. HRP-conjugated Streptavidin (MABTech 3310-9-1000) was added at a concentration of 1:4,000 and incubated for 1-hour shaking at RT. The HRP-substrate K-blue aqueous TMB (Neogen 331,177) was incubated on the plate for 1 min and the reaction was stopped by the addition of 1 M sulfuric acid. The signal intensity was measured as absorbance at 450 nm on the FLUOstar Omega microplate reader (BMG Labtech, Ortenberg, Germany) or on the TECAN Spark plate reader (Tecan, Männedorf, Switzerland). All antibody dilutions were prepared in ELISA incubation buffer (0.1% BSA, 0.05% Tween-20 in PBS), and wells were washed between each incubation with ELISA washing buffer (0.05% Tween-20 in PBS).

### Sandwich ELISA to assess cross-reactivity of HexaSynO2 and SynO2 toward Aβ42 aggregates

To investigate whether the additional binding sites on HexaSynO2 increase the reactivity to amyloids other than αSyn, we tested the binding of HexaSynO2 and SynO2 toward Aβ42 aggregates in a Sandwich ELISA. A high binding half-area 96-well plate (Corning CLS3690) was coated with a C-terminal Aβ42-specific antibody (Invitrogen 700,254) at a concentration of 1 µg/ml in PBS overnight at 4°C. After blocking the plates for 2 hours with 1% BSA (Sigma-Aldrich A7030) in PBS, cross-linked Aβ42 aggregates were added at a concentration of 10 nM in ELISA incubation buffer (0.1% BSA, 0.05% Tween-20 in PBS) and incubated for 2 hours shaking at RT. Serial dilutions of the antibodies in ELISA incubation buffer, with a starting



concentration of 10 nM, were incubated on the plates for 2-hour shaking at RT. Antibody binding was detected and read as described above.

### **Inhibition ELISA to discriminate the binding between $\alpha$ Syn monomers, $\alpha$ Syn HNE aggregates and $\alpha$ Syn fibrils**

Inhibition ELISA was performed to evaluate the differences in binding strength of HexaSynO2, TetraSynO2 and SynO2 to  $\alpha$ Syn monomers, soluble aggregates and fibrils. A high binding half-area 96-well plate (Corning CLS3690) was coated with  $\alpha$ Syn HNE aggregates at a concentration of 100 nM in PBS at 4°C over night and was blocked the next day with 1% BSA (Sigma-Aldrich A7030) in PBS for 2 hours shaking at RT. Serial dilutions of  $\alpha$ Syn monomers,  $\alpha$ Syn HNE aggregates and  $\alpha$ Syn fibrils, starting with 2000 nM of monomers or 200 nM of HNE aggregates and  $\alpha$ Syn fibrils, were pre-incubated with 500 pM of HexaSynO2, TetraSynO2 or SynO2 in low-binding plates for 1.5 hours shaking at RT. The pre-incubated antibody- $\alpha$ Syn samples were added to the  $\alpha$ Syn aggregates-coated plate and incubated for 15 min shaking at RT. Antibodies that were tightly bound to the  $\alpha$ Syn species in solution were washed off subsequently, while unbound antibodies or those with weaker binding to the  $\alpha$ Syn species in solution would be susceptible for binding to the  $\alpha$ Syn aggregates coating increasingly with decreasing concentration of  $\alpha$ Syn in the pre-incubation mixture. HRP-conjugated goat-anti-mouse antibody was added to detect antibodies bound to the plate and signals were developed and read as described above. IC<sub>50</sub> of  $\alpha$ Syn in solution, at which the antibody-binding to the coating was reduced by 50%, was calculated in GraphPad, where  $\alpha$ Syn concentrations were log transformed and the OD<sub>450</sub> values were normalized with OD<sub>450</sub> values of zero set as 0% binding and the highest OD<sub>450</sub> value, respectively, set as 100% binding. Linear regression curves were calculated using the “log(inhibitor) vs. normalized response” model.

### **Real-time interaction analysis with LigandTracer**

Association and dissociation rates of the antibodies to their target were determined using LigandTracer gray (Ridgeview Instruments, Uppsala, Sweden), which determines the amount of <sup>125</sup>I-labeled ligand binding to a surface-bound target by measuring the radioactivity in a defined “target area”, coated with the target, and a background area, located opposite to each other on a Petri dish. In the LigandTracer instrument, the Petri dish is placed on an inclined, rotating platform. Due to the incline, only the lower part of the Petri dish stays covered with the buffer. During a run, the platform rotates 180° every 30 seconds, alternating the incubation of the target area and the background with the buffer. The radioactivity is recorded in the upper part of the Petri dish which is not covered by buffer. 300  $\mu$ l of 100 nM  $\alpha$ Syn HNE aggregates in PBS were used to coat the target area on a Petri dish (Sarstedt 83.3902) overnight at 4°C. The next day, the coating solution was removed and the Petri dish was blocked with 5% BSA (Sigma-Aldrich A7030) in PBS for 2 hours at RT. The

**Table 1.** Start values for kinetic evaluations of interactions between antibodies and  $\alpha$ Syn HNE aggregates recorded by LigandTracer. All interaction curves were individually fit with start values set at <sup>(1)</sup> global scope or <sup>(2)</sup> constant scope as indicated below, respectively.

	$k_a1$ (M <sup>-1</sup> s <sup>-1</sup> )	$k_d1$ (s <sup>-1</sup> )	$k_a2$ (M <sup>-1</sup> s <sup>-1</sup> )	$k_d2$ (s <sup>-1</sup> )	nB	Vol (L)
SynO2Fab	1.0e5 <sup>(1)</sup>	1.0e-3 <sup>(1)</sup>	-	-	2e12 <sup>(1)</sup>	2.0e-3 <sup>(2)</sup>
SynO2	1.0e5 <sup>(1)</sup>	3.0e-4 <sup>(1)</sup>	3.0e5 <sup>(1)</sup>	1.0e-3 <sup>(1)</sup>	-	-
TetraSynO2	1.0e5 <sup>(1)</sup>	3.0e-6 <sup>(1)</sup>	1.0e5 <sup>(2)</sup>	2.37e-4 <sup>(2)</sup>	-	-
HexaSynO2	1.0e5 <sup>(1)</sup>	1.0e-3 <sup>(1)</sup>	-	-	2e12 <sup>(1)</sup>	2.0e-3 <sup>(2)</sup>

blocking solution was replaced by 2 ml 0.1% BSA in PBS. The Petri dish was placed in the LigandTracer and the background signal was measured for 10 min. The buffer was replaced by 2 ml 0.1% BSA where 1 nM <sup>125</sup>I-labeled antibody was added and the first association phase was run for 3 hours. A second association phase was performed with 3 nM <sup>125</sup>I labeled antibody for 4 hours followed by a dissociation phase overnight, where 2 ml 0.1% BSA in PBS without antibody was incubated on the plate. Overlay images, fitting curves and kinetic parameters were calculated with the TraceDrawer software (Ridgeview Instruments, Uppsala, Sweden). For the kinetic evaluation, start values for the respective kinetic parameters were set as summarized in Table 1. For easy visual comparison, signal intensities were scaled based on the estimated signal at saturation, Bmax (100/Bmax). The percentage of antibodies binding by avidity in the overall binding was calculated by Bmax1/(Bmax1+Bmax2), with Bmax1 representing the signal at saturation of the avidity enhanced interaction component and Bmax2 representing the signal at saturation of the weaker interaction component.

### **Abbreviations**

<sup>125</sup> I	Iodine-125
A $\beta$	amyloid beta
$\alpha$ Syn	alpha-Synuclein
Bmax	maximal binding capacity
BSA	bovine serum albumin
ELISA	enzyme-linked immuno assay
Fab	antigen-binding fragments
HMW	high molecular weight
HNE	4-hydroxynonenal
HRP	horseradish peroxidase
IC <sub>50</sub>	Half-maximal inhibitory concentrations
$k_a$	association rate constant
$k_d$	dissociation rate constant
KD	affinity
kDa	kilo dalton
MW	molecular weight
MWCO	molecular weight cutoff
PBS	phosphate-buffered saline
PD	Parkinson's disease
PEI	polyethyleneimine
red.	reducing
RT	room temperature
scFv	single-chain variable fragments
SDS-PAGE	Sodium dodecyl-sulfate polyacrylamide gel electrophoresis
SEC	size exclusion chromatography
SNARE	soluble N-ethylmaleimide-sensitive fusion protein attachment protein receptors
TBS	Tris-buffered saline
TEM	transmission electron microscopy



## Acknowledgments

Schematic illustrations were created with BioRender.com. We would like to acknowledge the Biophysical Screening and Characterization Unit at SciLifeLab for use of the Tycho NT.6 instrument.

## Disclosure statement

No potential conflict of interest was reported by the author(s).

## Funding

This work was supported by grants from Parkinsonsfonden, Swedish Research Council, Åhlén-stiftelsen, Jeanssonsfonderna, Magnus Bergvalls stiftelse, Vinnova, Alzheimerfonden, Stiftelsen Olle Engkvist Byggmästare, Bertil och Ebon Norlins stiftelse, Ingegerd Berghs stiftelse, Gunvor och Josef Aners stiftelse, O.E. och Edla Johanssonsfonden, Vetenskapsrådet and Torsten Söderbergs stiftelse.

## ORCID

Greta Hultqvist  <http://orcid.org/0000-0002-4136-6792>

## References

- Luo SX, Huang EJ. Dopaminergic neurons and brain reward pathways. *Am J Pathol.* 2016;186:478–88. doi:10.1016/j.ajpath.2015.09.023.
- Gibb WR, Lees AJ. The relevance of the Lewy body to the pathogenesis of idiopathic Parkinson's disease. *J Neurol Neurosurg Psychiatry.* 1988;51(6):745–52. doi:10.1136/jnnp.51.6.745.
- Bartels T, Choi JG, Selkoe DJ.  $\alpha$ -Synuclein occurs physiologically as a helically folded tetramer that resists aggregation. *Nature.* 2011;477:107–10. doi:10.1038/nature10324.
- Burré J, Sharma M, Südhof TC.  $\alpha$ -Synuclein assembles into higher-order multimers upon membrane binding to promote SNARE complex formation. *Proc Natl Acad Sci.* 2014;111(40):E4274–E83. doi:10.1073/pnas.1416598111.
- Killinger BA, Melki R, Brundin P, Kordower JH. Endogenous alpha-synuclein monomers, oligomers and resulting pathology: let's talk about the lipids in the room. *Npj Park Dis.* 2019;5(1):23. doi:10.1038/s41531-019-0095-3.
- Luth ES, Bartels T, Dettmer U, Kim NC, Selkoe DJ. Purification of  $\alpha$ -Synuclein from human brain reveals an instability of endogenous multimers as the protein approaches purity. *Biochemistry.* 2015;54(2):279–92. doi:10.1021/bi501188a.
- Cremades N, Cohen SIA, Deas E, Abramov AY, Chen AY, Orte A, Sandal M, Clarke RW, Dunne P, Aprile FA, et al. Direct observation of the interconversion of normal and toxic forms of  $\alpha$ -Synuclein. *Cell.* 2012;149(5):1048–59. doi:10.1016/j.cell.2012.03.037.
- de Oliveira GAP, Silva JL. Alpha-Synuclein stepwise aggregation reveals features of an early onset mutation in Parkinson's disease. *Commun Biol.* 2019;2(1):374. doi:10.1038/s42003-019-0598-9.
- Mirecka EA, Shaykhalishahi H, Gauhar A, Akgül Ş, Lecher J, Willbold D, Stoldt M, Hoyer W. Sequestration of a  $\beta$ -hairpin for control of  $\alpha$ -Synuclein aggregation. *Angew Chem Int Ed.* 2014;53(16):4227–30. doi:10.1002/anie.201309001.
- Salveson PJ, Spencer RK, Nowick JS. X-Ray crystallographic structure of oligomers formed by a toxic  $\beta$ -hairpin derived from  $\alpha$ -Synuclein: trimers and Higher-Order oligomers. *J Am Chem Soc.* 2016;138:4458–67. doi:10.1021/jacs.5b13261.
- Yu H, Han W, Ma W, Schulten K. Transient  $\beta$ -hairpin formation in  $\alpha$ -Synuclein monomer revealed by coarse-grained molecular dynamics simulation. *J Chem Phys.* 2015;143:243142. doi:10.1063/1.4936910.
- Celej MS, Sarroukh R, Goormaghtigh E, Fidelio GD, Ruyschaert J-M, Raussens V. Toxic prefibrillar  $\alpha$ -Synuclein amyloid oligomers adopt a distinctive antiparallel  $\beta$ -sheet structure. *Biochem J.* 2012;443:719–26. doi:10.1042/BJ20111924.
- Kim H-Y, Cho M-K, Kumar A, Maier E, Siebenhaar C, Becker S, Fernandez CO, Lashuel HA, Benz R, Lange A, et al. Structural properties of pore-forming oligomers of  $\alpha$ -Synuclein. *J Am Chem Soc.* 2009;131(47):17482–89. doi:10.1021/ja9077599.
- Cascella R, Chen SW, Bigi A, Camino JD, Xu CK, Dobson CM, Chiti F, Cremades N, Cecchi C. The release of toxic oligomers from  $\alpha$ -Synuclein fibrils induces dysfunction in neuronal cells. *Nat Commun.* 2021;12(1):1814. doi:10.1038/s41467-021-21937-3.
- Fusco G, Chen SW, Williamson PTF, Cascella R, Perni M, Jarvis JA, Cecchi C, Vendruscolo M, Chiti F, Cremades N, et al. Structural basis of membrane disruption and cellular toxicity by  $\alpha$ -Synuclein Oligomers. *Sci.* 2017;358(6369):1440–43. doi:10.1126/science.aan6160.
- Choi B-K, Choi M-G, Kim J-Y, Yang Y, Lai Y, Kweon D-H, Lee NK, Shin Y-K. Large  $\alpha$ -synuclein oligomers inhibit neuronal SNARE-mediated vesicle docking. *Proc Natl Acad Sci.* 2013;110(10):4087–92. doi:10.1073/pnas.1218424110.
- Deas E, Cremades N, Angelova PR, Ludtmann MHR, Yao Z, Chen S, Horrocks MH, Banushi B, Little D, Devine MJ, et al. Alpha-Synuclein oligomers interact with metal ions to induce oxidative stress and neuronal death in Parkinson's disease. *Antioxid Redox Signal.* 2016;24(7):376–91. doi:10.1089/ars.2015.6343.
- Di Maio R, Barrett PJ, Hoffman EK, Barrett CW, Zharikov A, Borah A, Hu X, McCoy J, Chu CT, Burton EA, et al.  $\alpha$ -Synuclein binds to TOM20 and inhibits mitochondrial protein import in Parkinson's disease. *Sci Transl Med.* 2016;8. doi:10.1126/scitranslmed.aaf3634.
- Ludtmann MHR, Angelova PR, Horrocks MH, Choi ML, Rodrigues M, Baev AY, Berezhnov AV, Yao Z, Little D, Banushi B, et al.  $\alpha$ -Synuclein oligomers interact with ATP synthase and open the permeability transition pore in Parkinson's disease. *Nat Commun.* 2018;9:2293. doi:10.1038/s41467-018-04422-2.
- Daniele SG, Béraud D, Davenport C, Cheng K, Yin H, Maguire-Zeiss KA. Activation of MyD88-dependent TLR1/2 signaling by misfolded  $\alpha$ -Synuclein, a protein linked to neurodegenerative disorders. *Sci Signal.* 2015;8. doi:10.1126/scisignal.2005965.
- Lee H-J, Suk J-E, Patrick C, Bae E-J, Cho J-H, Rho S, Hwang D, Masliah E, Lee S-J. Direct Transfer of  $\alpha$ -Synuclein from neuron to astroglia causes inflammatory responses in synucleinopathies. *J Biol Chem.* 2010;285:9262–72. doi:10.1074/jbc.M109.081125.
- Emmanouilidou E, Melachroinou K, Roumeliotis T, Garbis SD, Ntzouni M, Margaritis LH, Stefanis L, Vekrellis K. Cell-produced  $\alpha$ -Synuclein is secreted in a calcium-dependent manner by exosomes and impacts neuronal survival. *J Neurosci.* 2010;30(20):6838–51. doi:10.1523/JNEUROSCI.5699-09.2010.
- Lee H-J, Kim C, Lee S-J. Alpha-Synuclein stimulation of astrocytes: potential role for neuroinflammation and neuroprotection. *Oxid Med Cell Longev.* 2010;3:283–87. doi:10.4161/oxim.3.4.12809.
- Lee H-J, Suk J-E, Bae E-J, Lee S-J. Clearance and deposition of extracellular  $\alpha$ -Synuclein aggregates in microglia. *Biochem Biophys Res Commun.* 2008;372(3):423–28. doi:10.1016/j.bbrc.2008.05.045.
- Brahic M, Bousset L, Bieri G, Melki R, Gitler AD. Axonal transport and secretion of fibrillar forms of  $\alpha$ -Synuclein, A $\beta$ 42 peptide and HTTExon 1. *Acta Neuropathol (Berl).* 2016;131(4):539–48. doi:10.1007/s00401-016-1538-0.
- Rey NL, Petit GH, Bousset L, Melki R, Brundin P. Transfer of human  $\alpha$ -Synuclein from the olfactory bulb to Interconnected brain regions in mice. *Acta Neuropathol (Berl).* 2013;126(4):555–73. doi:10.1007/s00401-013-1160-3.
- Fjord-Larsen L, Thougard A, Wegener KM, Christiansen J, Larsen F, Schröder-Hansen LM, Kaarde M, Ditlevsen DK. Nonclinical safety evaluation, pharmacokinetics, and target engagement of Lu AF82422, a monoclonal IgG1 antibody against alpha-Synuclein in development for treatment of



- synucleinopathies. *MAbs*. 2021;13(1):1994690. doi:10.1080/19420862.2021.1994690.
28. Kalluri H, Zadikoff C, Rueter L, Graff O, Xiong H. Randomized, placebo-controlled single ascending dose study to evaluate the safety, tolerability, pharmacokinetics, and immunogenicity of ABBV-0805, an anti- $\alpha$ -Synuclein monoclonal antibody in healthy subjects [abstract]. *Mov Disord*. 2021;36. doi:10.1002/mds.28794.
  29. Lang AE, Siderowf AD, Macklin EA, Poewe W, Brooks DJ, Fernandez HH, Rascol O, Giladi N, Stocchi F, Tanner CM, et al. Trial of cinpanemab in early Parkinson's disease. *N Engl J Med*. 2022;387(5):408–20. doi:10.1056/NEJMoa2203395.
  30. Pagano G, Taylor KI, Anzures-Cabrera J, Marchesi M, Simuni T, Marek K, Postuma RB, Pavese N, Stocchi F, Azulay J-P, et al. Trial of prasinezumab in early-stage Parkinson's disease. *N Engl J Med*. 2022;387(5):421–32. doi:10.1056/NEJMoa2202867.
  31. Schofield DJ, Irving L, Calo L, Bogstedt A, Rees G, Nuccitelli A, Narwal R, Petrone M, Roberts J, Brown L, et al. Preclinical development of a high affinity  $\alpha$ -Synuclein antibody, MEDI1341, that can enter the brain, sequester extracellular  $\alpha$ -Synuclein and attenuate  $\alpha$ -Synuclein spreading in vivo. *Neurobiol Dis*. 2019;132:104582. doi:10.1016/j.nbd.2019.104582.
  32. Roshanbin S, Julku U, Xiong M, Eriksson J, Masliah E, Hultqvist G, Bergström J, Ingelsson M, Syvänen S, Sehlin D. Reduction of ASYN pathology in a mouse model of PD using a brain-penetrating bispecific antibody. *Pharmaceutics*. 2022;14(7):1412. doi:10.3390/pharmaceutics14071412.
  33. Oliveira LMA, Gasser T, Edwards R, Zweckstetter M, Melki R, Stefanis L, Lashuel HA, Sulzer D, Vekrellis K, Halliday GM, et al. Alpha-Synuclein Research: defining strategic moves in the battle against Parkinson's disease. *Npj Park Dis*. 2021;7(1):65. doi:10.1038/s41531-021-00203-9.
  34. Rofo F, Meier SR, Metzendorf NG, Morrison JI, Petrovic A, Syvänen S, Sehlin D, Hultqvist G. A brain-targeting bispecific-multivalent antibody clears soluble amyloid-beta aggregates in Alzheimer's disease mice. *Neurotherapeutics*. 2022;19(5):1588–602. doi:10.1007/s13311-022-01283-y.
  35. Rofo F, Buijs J, Falk R, Honek K, Lannfelt L, Lilja AM, Metzendorf NG, Gustavsson T, Sehlin D, Söderberg L, et al. Novel multivalent design of a monoclonal antibody improves binding strength to soluble aggregates of amyloid beta. *Transl Neurodegener*. 2021;10(1):38. doi:10.1186/s40035-021-00258-x.
  36. van Dyck CH, Swanson CJ, Aisen P, Bateman RJ, Chen C, Gee M, Kanekiyo M, Li D, Reyderman L, Cohen S, et al. Lecanemab in early Alzheimer's disease. *N Engl J Med*. 2023;388(1):9–21. doi:10.1056/NEJMoa2212948.
  37. Vaikath NN, Majbour NK, Paleologou KE, Ardah MT, van Dam E, van de Berg WDJ, Forrest SL, Parkkinen L, Gai W-P, Hattori N, et al. Generation and Characterization of novel conformation-specific monoclonal antibodies for  $\alpha$ -Synuclein pathology. *Neurobiol Dis*. 2015;79:81–99. doi:10.1016/j.nbd.2015.04.009.
  38. Castonguay A-M, Gravel C, Lévesque M. Treating Parkinson's disease with antibodies: previous studies and future directions. *J Park Dis*. 2021;11(1):71–92. doi:10.3233/JPD-202221.
  39. Morrison JI, Metzendorf NG, Rofo F, Petrovic A, Hultqvist G. A single chain fragment constant (scFc) design enables easy production of a monovalent BBB transporter and provides an improved brain Uptake at elevated doses. *J Neurochem*. 2023;15768. doi:10.1111/jnc.15768.
  40. Bondza S, ten Broeke T, Nestor M, Leusen JHW, Buijs J. Bivalent binding on cells varies between anti-CD20 antibodies and is dose-dependent. *MAbs*. 2020;12(1):1792673. doi:10.1080/19420862.2020.1792673.
  41. Kumar ST, Jagannath S, Francois C, Vanderstichele H, Stoops E, Lashuel HA. How specific are the conformation-specific  $\alpha$ -Synuclein antibodies? Characterization and validation of 16  $\alpha$ -Synuclein conformation-specific antibodies using well-characterized preparations of  $\alpha$ -Synuclein monomers, fibrils and oligomers with distinct structures and morphology. *Neurobiol Dis*. 2020;146:105086. doi:10.1016/j.nbd.2020.105086.
  42. Yusakul G, Sakamoto S, Pongkitwitoon B, Tanaka H, Morimoto S. Effect of Linker length between variable domains of single chain variable fragment antibody against Daidzin on its reactivity. *Biosci Biotechnol Biochem*. 2016;80:1306–12. doi:10.1080/09168451.2016.1156482.
  43. Fang XT, Sehlin D, Lannfelt L, Syvänen S, Hultqvist G. Efficient and inexpensive transient expression of multispecific multivalent antibodies in Expi293 cells. *Biol Proced Online*. 2017;19(1):11. doi:10.1186/s12575-017-0060-7.
  44. Almandoz-Gil L, Welandar H, Ihse E, Khoonsari PE, Musunuri S, Lendel C, Sigvardson J, Karlsson M, Ingelsson M, Kultima K, et al. Low molar excess of 4-oxo-2-nonenal and 4-hydroxy-2-nonenal promote oligomerization of alpha-Synuclein through different pathways. *Free Radic Biol Med*. 2017;110:421–31. doi:10.1016/j.freeradbiomed.2017.07.004.
  45. Hunter WM, Greenwood FC. Preparation of Iodine-131 labelled human growth hormone of high specific activity. *Nature*. 1962;194(4827):495–96. doi:10.1038/194495a0.